Positive Pressure Induced Channeled Suction Cups

by

Shannon X. Yang

Submitted to the Department of Mechanical Engineering
in Partial Fulfillment of the Requirements for the Degree of
Bachelors of Science in Mechanical Engineering

at the
Massachusetts Institute of Technology
June, 2013

Signature of Author.....
Department of Mechanical Engineering
May 24th 2013

Certified by.....
Sangbae Kim
Assistant Professor of Mechanical Engineering
Thesis Supervisor

Accepted by.....
Anette Hosoi
Professor of Mechanical Engineering
Undergraduate Officer

Positive Pressure Induced Channeled Suction Cups

by

Shannon Yang

Submitted to the Department of Mechanical Engineering

on June, 2013 in Partial Fulfillment of the

Requirements for the Degree of Master of Science in

Mechanical Engineering

ABSTRACT

Leaking in water pipe is a critical issue in Middle Eastern countries such as Kuwait where water is scarce. In-pipe robots can be dispatched to discover the network and inspect the inner surface of the pipe. This thesis describes the design and characterization of suction pads for in-pipe robots. The suction cups are made of hyperelastic materials that contain air channels inside. Instead of using conventional suction technique that is prone to leaking and loosing adhesion force, the suction cup is actuated by compressed air or liquid, which deforms the geometry of the cup to achieve suction. In order to verify the geometry changes during actuation, a uniaxial tension test was done on the elastic material used to acquire the material properties and the suction cup designs were then simulated using FEA in ABAQUS. Next, prototypes were designed in SolidWorks and fabricated using soft lithography techniques. To measure the suction force, pressure measurements were taken both inside the prototype channels and underneath the suction cup. Results show that a Positive Pressure Actuated Suction-cup (PPAS) of diameter forty millimeters can achieve suction force up to 68 N. As more air is inserted into PPAS, the suction force also increases. The concept has proved to be a feasible solution for pipe inspection robot.

Thesis Supervisor: Sangbae Kim

Title: Assistant Professor of Mechanical Engineering

ACKNOWLEDGEMENTS

I would like to offer my special thanks to Professor Sangbae Kim for his advice and support throughout the course of this project. Professor Kim has made himself available whenever I have asked for his time and been very patient with me throughout this year. He has been both a mentor and an inspiration for me to become a better student and researcher.

Coming into this lab has been a surprise and a blessing. It was the first step for me to enter into a team of researchers and understand how a lab can truly be a family and support each other on a day to day basis. I wish to acknowledge Albert Wang for his advice in LabView, teaching me CNC, and his ever-optimistic personality. I would like to thank Michael Chuah for his assistance in prototype manufacturing and his laughter that brightened up everyone's day. I'd also like to shout out to Claudio Di Leo for his extensive assistance in ABAQUS. I am particularly grateful to my supervisor, Yichao Pan for his guidance and encouragement. Though sometimes Yichao and I did not see eye to eye, I have never doubted for the slightest bit that Yichao wanted to be the best mentor for me, and he was. My special thanks to Dr. Haewon Park and Sangok Seok for their encouragement and genuine acceptance of me to become a part of the family.

It has been such an honor to be working the MIT Biomimetics team. The people here make this place so special and I will always consider 5-017 to be a second home, forever dear to my heart.

CONTENTS

FIGURES

TABLES

Chapter

1

INTRODUCTION

1.1 Motivation

Water pipe inspection is becoming an important issue as we lose more freshwater. In the countries where natural fresh water is scarce, the pipe maintenance is particularly critical. More than 90% of the water supply in the State of Kuwait is dependent on non-conventional water sources such as seawater desalination, as it has very limited rainfall and natural ground water. The water is transferred underground by their large water pipeline network (WPN), where reportedly large leakage occurs. In addition, the original documentation of WPN map has not been updated, so there is a lack of explicit layout of internal structure of the network. Because the WPN is largely underground, the only easy access point to both map and examine the condition of the pipes is from inside the pipes.

In order to access from inside the pipeline, our approach is to develop an autonomous robot capable of discovering and mapping the existing WPN and to provide explicit eye-views of the internal structure of the pipeline network. Because water flow cannot be interrupted even during pipe maintenance, procedures of robot inspection cannot interfere with normal pipeline function. Moreover, the robot must be able to maneuver both with and against water flow.

There have been extensive prototypes and research on the topic of pipe-inspection robots. Many robots are wheeled robots that induce a radial load on the inner surface of the pipe to create traction such that when the wheels are rolling, the robot moves along the pipe [1]. Some disadvantages of wheeled robots include 1) they are typically designed for a specific pipe size

and are unable to accommodate a range of pipe sizes and 2) they take up a large portion of the pipe cross section area and have disadvantages when traveling against flow. The WPN in Kuwait have pipe diameters varying from 150 mm to 800 mm, so the pipe-inspection robot must be able to secure traction accommodating the entire range of pipe diameters.

Because there is need to securely attach the robot to pipe surface, suction is chosen as the method of temporary attachment, in other words, the mechanism to acquire traction, during robot locomotion. Suction cups are made of rubbery materials, which are flexible and can conform to the curved surfaces of pipes. In addition suction force can also be tuned to a desired magnitude depending on the need. Active suction cups are typically powered by a pump that sucks the air underneath the cup out. However, pumps used for similar applications are usually heavy and large in size; for this reason, we investigate the use of compressive hydraulic as an alternative actuation method. Whereas conventional suction needs high power due to leakage, compressive hydraulic is preferred in small robots because small displacements are necessary.

1.2 Background

1.2.1 Past Pipe Inspection Robots

Many in-pipe robots have been studied recently as a mobile carrier for visual inspection and nondestructive testing to pipe corrosion, crack, defect, and wall thickness of main gas pipelines [1]. Locomotion mechanisms that have been used for in-pipe robots include, but are not limited to wheeled type, snaking type, walking type, and worming type. Most prototypes up to date are designed for one size pipe diameter [2][3][4][5][6][7]. Recently, a few wheeled robots that are able to adapt to a limited range of varying pipe diameters have been developed [1][8]. A big challenge in in-pipe robots is to acquire enough traction against the pipe wall surface. Most in-pipe robots are designed with wheels 120 degrees apart contacting the inner surface of the pipes. The wheels provide a normal force that gives traction against the pipe walls and rolls to thrust the robot body forward. Another challenge in pipe inspection robots is the power supply. Whereas few designs are self-contained [9], many are tethered [7]. There are few legged in-pipe robots that use crawling as a method of locomotion. However, there are many studies of robots that utilize various attachment methods, such as Van der Waals forces [10] or suction forces [11] as a means of temporary adherence during locomotion.

1.2.2 Passive and Active Suction Cups

There are two types of suction cups, passively and actively actuated. Both types are made of nonporous materials. They are first pushed on to a surface to 1) release a portion of the gas fluid under the cup and 2) establish contact and seal around the circumferential area. The stiffness of the suction cup material tends to restore the deformed suction cup to its original shape, which causes the volume under the suction cup to increase and pressure to decrease inside the suction cup. The lower pressure in the cup compared to atmospheric pressure outside the cup causes a suction force to attach the cup to the contact surface. The suction force acquired is expressed in the equation below:

$$F_{suction} = (P_{in} - P_{atm})A_c \tag{1.1}$$

Where P_{in} is the pressure inside the cup, and P_{atm} is atmospheric pressure and A_c is the cross section area of the suction cup.

For an active suction cup, the same theory applies. Though instead of pushing the gas fluid out when the suction cup makes contact with the surface, a pump is used to pull gas out from within the cup to create a negative pressure.

There are several robots using suction as the locomotion or grasping mechanism. Both passive and active suction cups are utilized; however, many use active suction to gain more control over the mechanism.

1.2.3 Using Elastomeric Polymers for Pneumatically Actuated Robot Locomotion

Currently, there are many soft robot [12] projects that use various types of silicon rubber and polyurethane in portions of the robot to provide flexibility at joints. There have also been few robots that use elastomers as a method of attachment [13][14]. The multigait soft robot [15] was one of the first to use pneumatic actuation to create movement in the soft robot. This robot is made silicon rubber and PDMS using soft lithography. The robot is made of a series of chambers embedded in a layer of extensible elastomer and bonded to an inextensible layer. The chambers inflate during pneumatic actuation and cause the robot body to be largely deformed. The variation in the number of chambers, their orientation, and size allows control of the curvature of

the robot during bending of robot limbs. The cross section chambers are rectangular in shape and are laid out perpendicular to the bending curvature. This forms a 2-D deformation.

The PPAS is inspired by the same idea of using pneumatic actuation to deform a suction cup in a 3-dimensional way, such that a flat plane is morphed into a hemisphere shape. Using deformation to create a larger volume under the suction cup hemisphere, PPAS is able to decrease the pressure under the cup, creating a pressure differential to achieve suction.

First PPAS must first come in contact with a surface that allows the flaps of the PPAS to have a ring of contact and establish seal. Then, air is inserted into PPAS through the stem and allows the system to expand. The top surface is thinner than the bottom surface and therefore experiences more expansion. As shown in Figure 2.1, the rectangular-shaped cross section channels deforms to a round trapezoidal-shaped cross section. The positive pressure inside the channels puts on an expansion load to the elastomer and causes the volume under the cup to increase, therefore decreasing the pressure.

Chapter

2

HYPOTHESIS AND PROTOTYPE

2.1 Hypothesis

The PPAS is composed of two types of materials, Ecoflex 00-30 and VytaFlex 60, as shown in Table 2.1. The geometry and the stiffness of the two materials is what cause PPAS to deform. Because the stiffness of the two materials used and the thickness variation (where the base is significantly greater than the thickness between the channels and the thickness of top surface), when gaseous fluid is inserted into the channels of the suction cup, the cup deforms from a near flat circular pad into a hemisphere shape. Figure 2.1 illustrates the theoretical geometry deformation of the suction during actuation.

Table 2.1: Material Properties

Material	Shore A Hardness (ASTM D-2240)	Tensile Strength (ASTM D-412)	Elongation at Break %
EcoFlex 00-30	00-30	200 psi	900%
VytaFlex 60	60A	880 psi	480%

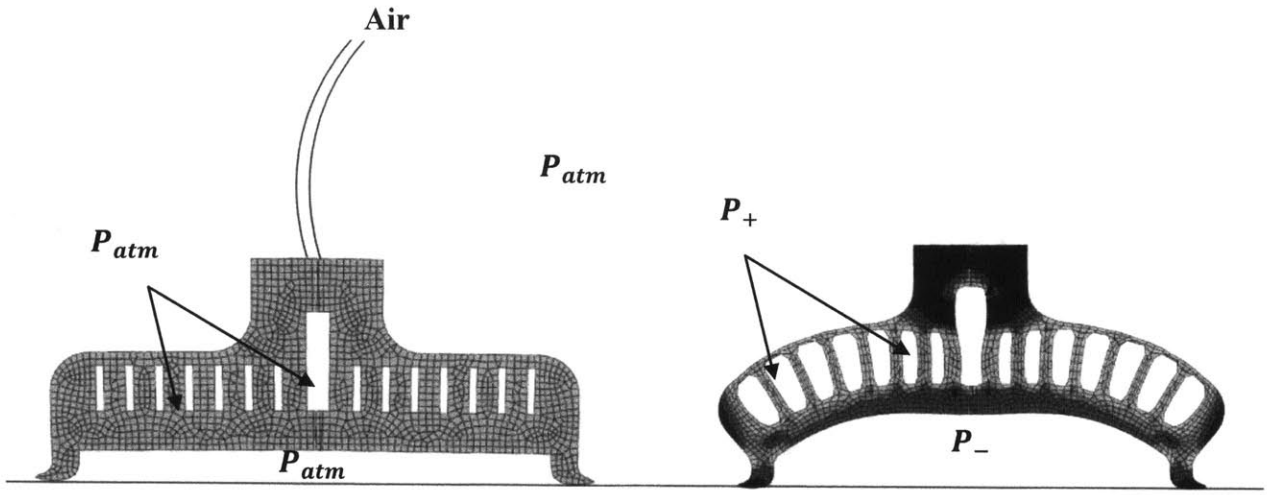

Figure 2.1: Hypothesis on inital and deforemd PPAS

2.2 FEA Simulation in ABAQUS

Due to the complex geometry and the use of highly-nonlinear hyperelastic material, a constitutive derivation for the PPAS deformation was not resolved. Instead, models were created and analyzed using Finite Element Analysis (FEA) in ABAQUS 6.10. The goal of the FEA simulation is to check both the behavior of the geometry and estimate the suction force created when certain amount of air is inserted to cause a positive pressure differential.

Many mathematical models have been explored and established for modeling highly non-linear elastomers. Because deformation causes the material to be strained to more than 35% [16], a constitutive model is not described. The Neo-Hookean model is based on statistical thermodynamics of cross-linked polymer chains and is typically used to describe rubber-like materials in the linear states [17][20]. However, it does not predict material behavior at large deformation. The Mooney-Rivlin model [18] was chosen for this highly nonlinear simulation. The Mooney-Rivlin model is a hyperelastic material model that is known to predict hyper-elasticity with local values of strains up to about 200% [19]. The strain energy density function for an incompressible Mooney-Rivlin model is described as:

$$W = C_{10}(\overline{I_1} - 3) + C_{01}(\overline{I_2} - 3) \tag{2.1}$$

Where C_{10} and C_{01} are material constants determined empirically and $\overline{I_1}$ and $\overline{I_2}$ are the first and second invariant of the deviatoric component of the left Cauchy-Green deformation tensor. The material constants were obtained using the following two equations:

$$\mu = 2(C_{10} + C_{01}) \tag{2.2}$$

$$\kappa = \frac{2(c_{10} + C_{01})}{1 - 2\nu} \tag{2.3}$$

Where μ is the initial shear modulus, κ is the initial bulk modulus, and ν is the poissons ratio of the material (commonly$\nu \cong 0.5$, for an incompressible rubber material). Table 2.2 describes the material property used to acquire C_{10} and C_{01}used in the FEA analysis.

Table 2.2: Mechanical Properties, Dimensions and Meshing Elements for Silicone Rubber [20]

Silicone Rubber	Initial shear modulus (μ) (MPa)	Initial bulk modulus (κ)(MPa)	Dimensions (mm)
Ecoflex 00-30	0.009542	0.106017	37.47x 8.12 x5.3

Using poissons ratio $\nu = 0.499$ and the initial shear modulus and the initial bulk modulus shown in Table 2.1 and Equations 2.2 and 2.3, the material properties are obtained to be $C_{10} = 7.103$ KPa and $C_{01} = 2.332$ KPa In addition, the material is modeled to be incompressible in volume. Using these coefficients, material is stable at all strains.

The pressure inside the channels was first measured using a pressure sensor (see detailed description in Chapter 3) and used as input load in simulation. The channel load is defined as a uniform, static, pressure differential of 20 KPa. This is the maxim pressure achieved and measured in the channels (four-petal prototype) when 10 mL of air was inserted into the prototype. Boundary conditions specified that the model is axisymmetric and the flap is not translating in x, y, or z direction. This is analogous to having a perfect seal with the contact surface.

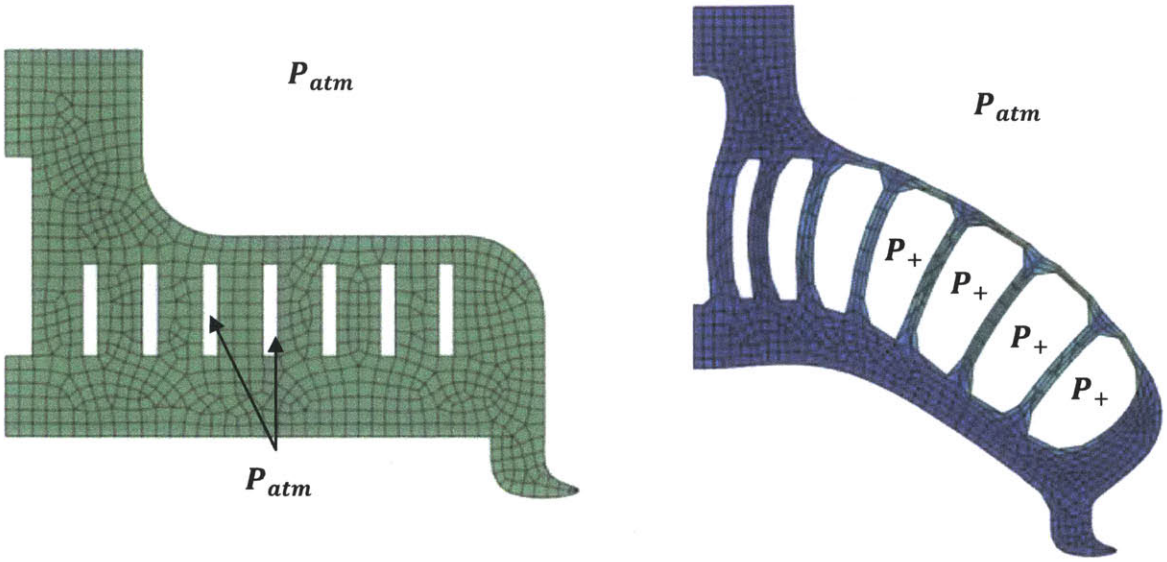

Figure 2.2: FEA analysis in ABAQUS showing un-deformed (left) and deformed states with 10 mL of air inserted as actuation

As shown in Figure 2.2, each cross section channel of the PPAS expands more on the top than the bottom due to the difference in thickness and causes the whole shape to become more like a bowl shape. With a pressure differential of 20 KPa, the von-misses stress experienced by the deformed PPAS ranges from 0-3.594 MPa. A large portion of the geometry (shown in blue) experiences von-misses stress less than 10 Pa. As expected, the largest stress occurs on the top surface and walls between the channels. The principle strain experienced is depicted in Figure 2.3. The strain range experienced goes from -0.005 to 1.094.

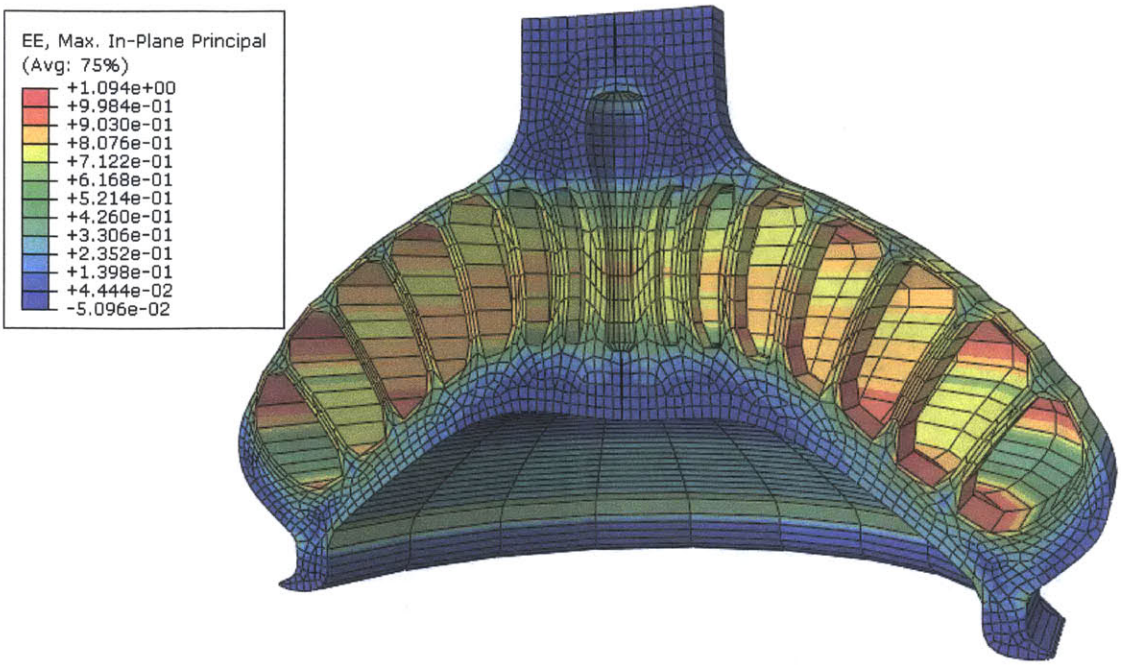

Figure 2.3: FEA analysis of 4 - petal prototype in ABAQUS

To verify the material coefficients used in the FEA analysis, a uniaxial tension test was done on a single specimen. To perform a unidirectional tension test, the sample is clamped in the Instron machine and tightened using a wrench. The Instron machine samples and records the time since start of one test cycle, the tension force and elongation experienced by the sample elastic. The Instron test set up is shown in Figure 2.4.

Two monitors were used in the experiment: one to control the Instron 5582 machine using the Instron Bluehill software and another for running the Vic-Snap software, as shown in Figure 2.5. Vic-Snap is a system that uses digital imaging to make strain measurements. An AF Micro Nikkor 60mm lens was used to capture a series of digital images of the specimen during the testing process. Though the software is capable of DIC, analyzing the difference between pixels of consecutive images to correlate them and create a strain map; this function was not used for this experiment. Vic-Snap was only used for taking a series of pictures and correlating them to the force and elongation data points. The pictures are shown in Figure 2.6.

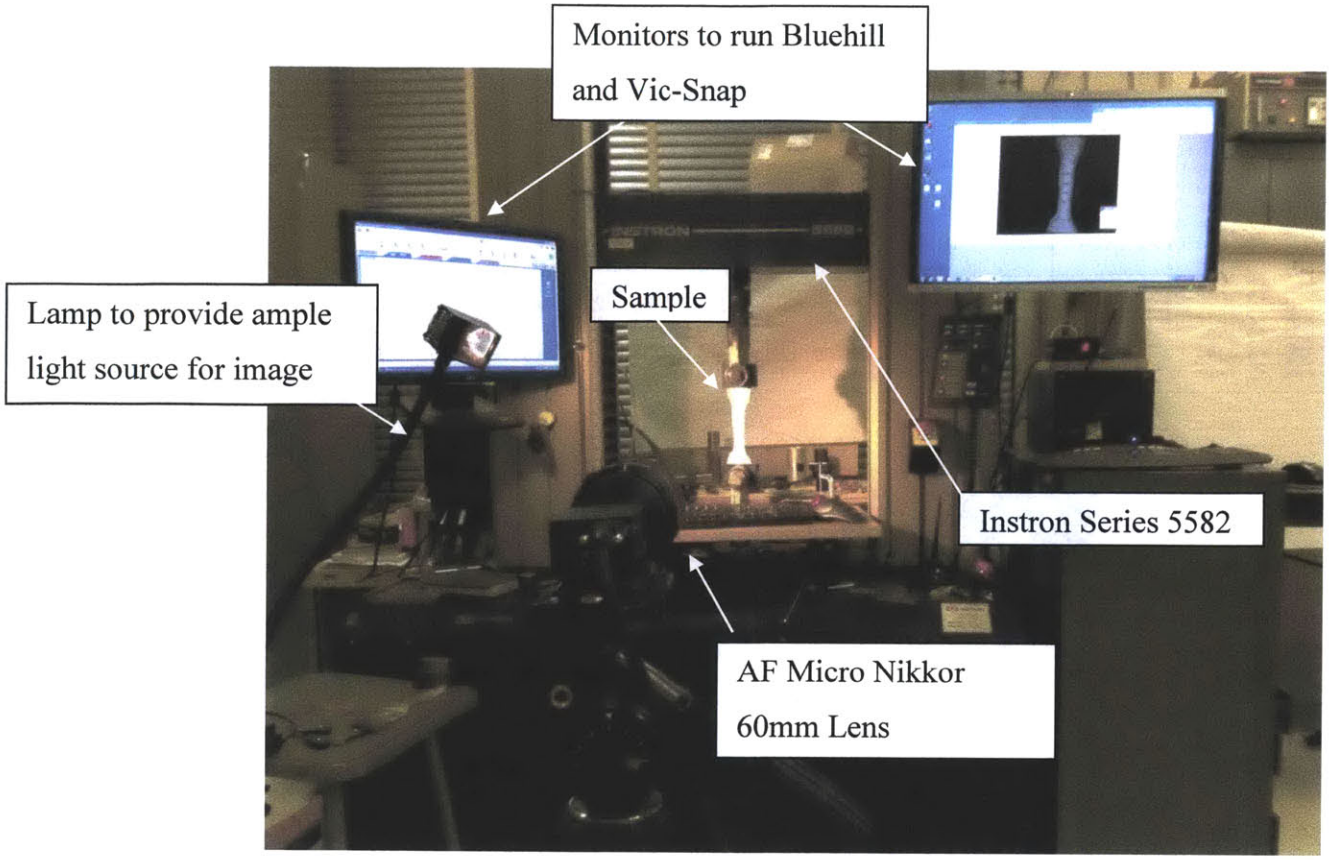

Figure 2.4: Test set-up for uniaxial tension test

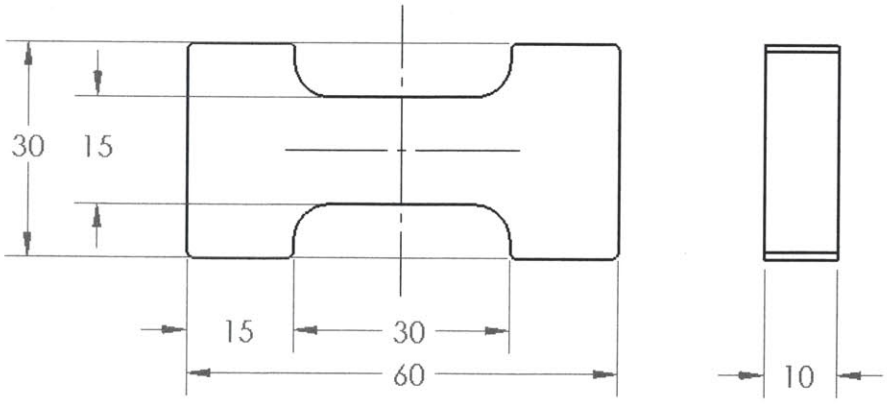

Figure 2.5: Test sample dimension (mm)

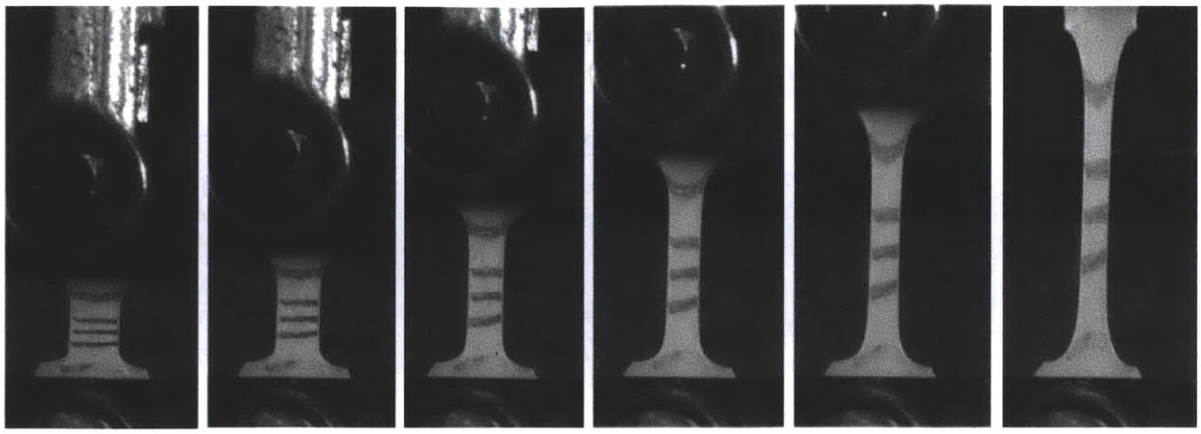

0 N 8 N 16 N 24 N 32 N 46 N

Figure 2.6: Uniaxial test on Instron machine of Ecoflex00-30 specimen

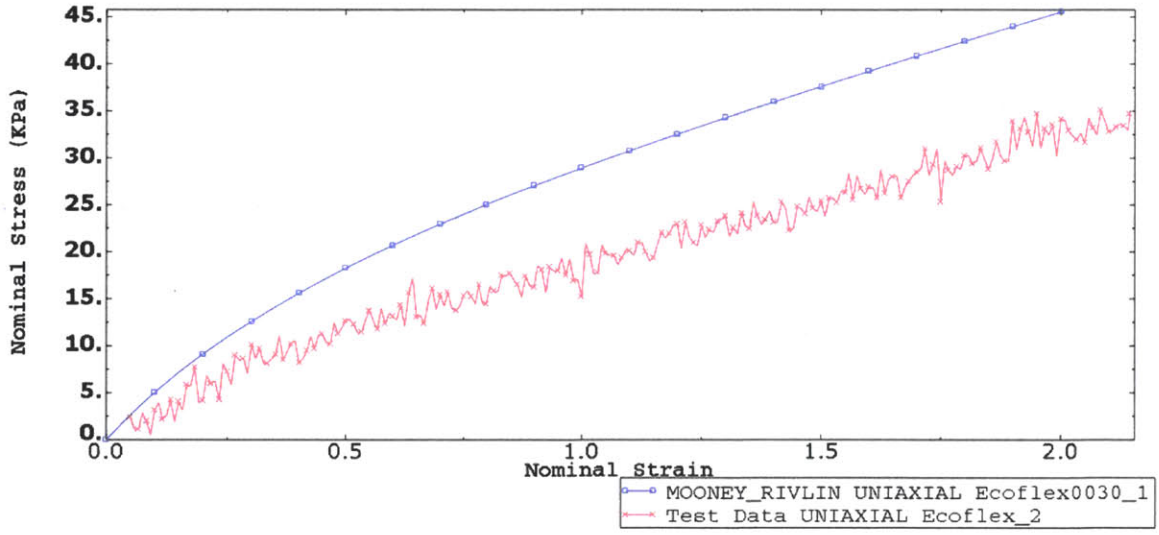

Figure 2.7: Comparison of derived coefficients and uniaxial tension data

The uniaxial tension test data was then graphed with the Mooney-Rivlin model plotted using the coefficients $C_{10} = 7.103$ KPa and $C_{01} = 2.332$ KPa. As shown, there is a significant error in test data and derived coefficients. The uniaxial tension test was evaluated in ABAQUS and plotted below in Figure 2.8. Polynomial fits of strain energy potential of order 1 and 2 are fitted. The models are simulated using the material coefficients represented by polynomial fit of strain energy potential of order 1—the Mooney-Rivlin model. Table 2.2 shows the material parameters and stability limit information obtained from the uniaxial data. The material coefficients and stability limits are calculated using the Mooney-Rivlin model and shown in

Table 2.3. The strain range experienced, according to the FEA analysis from ABAQUS, falls in the stable region

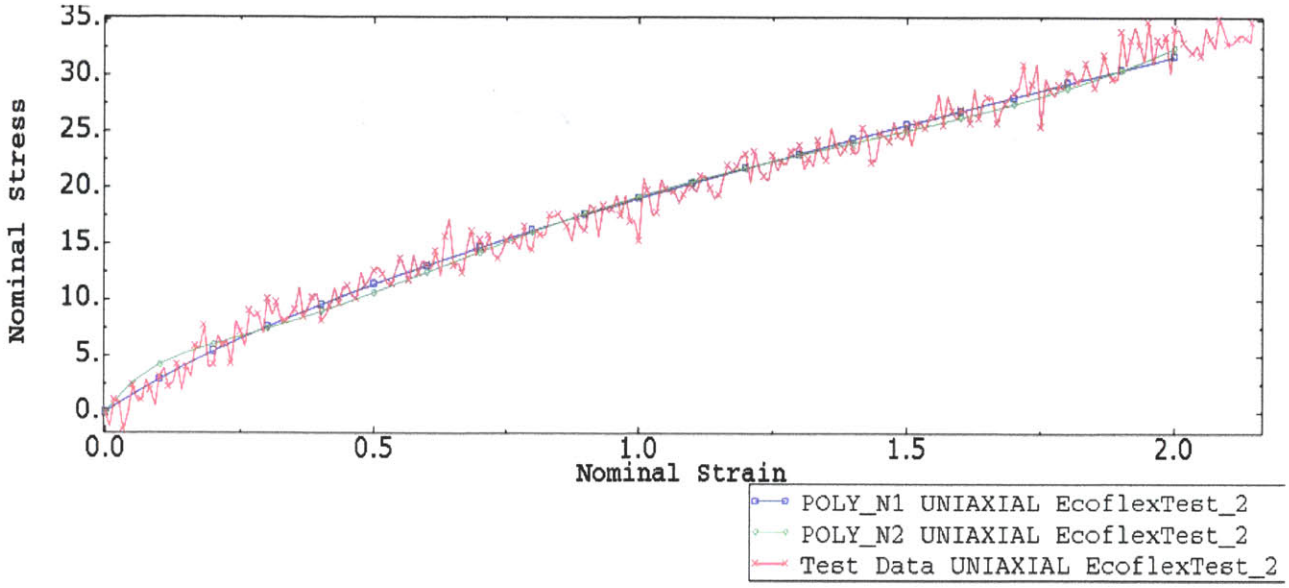

Figure 2.8: Uniaxial tension test evaluated for Mooney-Rivlin Coefficients

Table 2.3: Material Coefficients and Stability Limits Analyzed from Uniaxial Tension Test

Material Coefficients	
C_{10}	5569.12
C_{01}	-269.79
Stability:	
Uniaxial tension limit	3.55
Uniaxial compression limit	-0.90
Biaxial tension limit	2.22
Biaxial compression limit	-0.53
Planar tension limit	3.45
Planar compression limit	-0.78

Using the evaluated coefficients in ABAQUS, the model was analyzed again. The results are shown in Figure 2.9. We can see from results that the strain experienced ranges from approximately 3% in compression to 75% in tension. Both are within the stable range of the coefficients used.

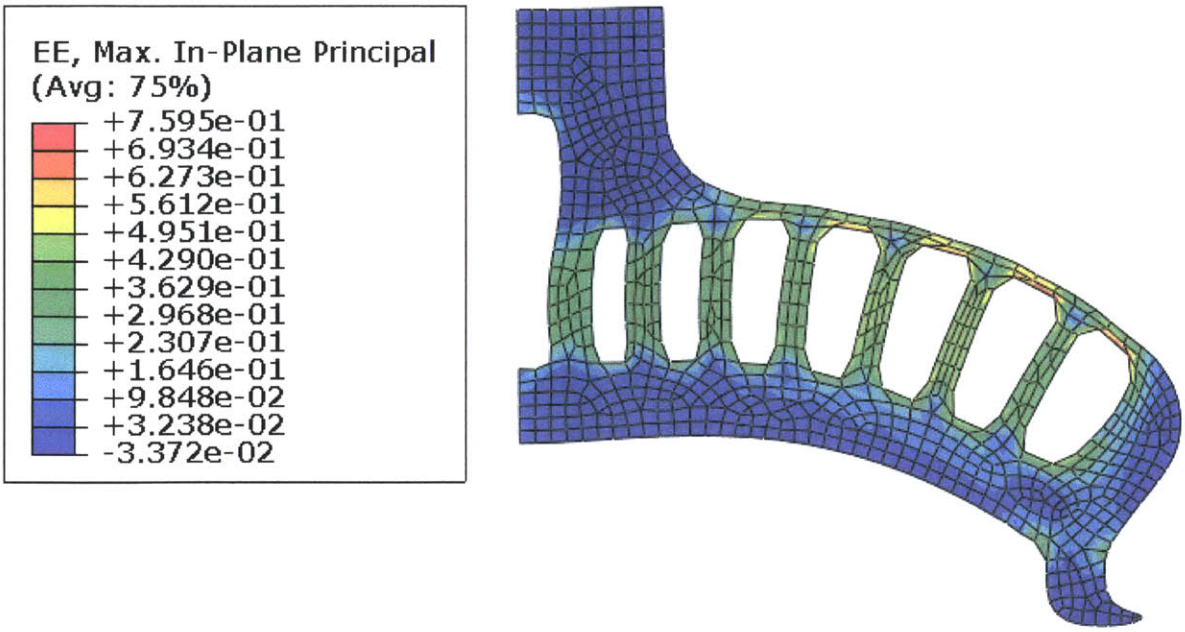

Figure 2.9: FEA analysis of four-petal prototype in ABAQUS using test evaluated coefficients

2.3 Prototype Fabrication

Three different PPAS prototypes were made given the available manufacturing processes. For each prototype, the mold was either 3D printed in ABS or CNC machined in delrin. All prototypes were over-molded multiple times in order to successfully fabricate the complex geometry.

The three prototypes differ in geometry and size. Table 2.4 describes the dimensions and characteristics of the prototypes. The cross-section area describes the size of the PPAS from top view and the channel volume describes volume at initial state, without any deformation. The deformation area is the area projected by the channels onto the top face of PPAS.

Table 2.4: Prototype Characteristics

Prototype	Cross-section Area (mm^2)	Channel Volume(mm^3)	Deformation Area (mm^2)
1-4 Petals	40	937.48	253.71
2-Spiral	40	905.33	292.45
3-2Flap	47.2	937.48	253.71

2.3.1 Prototype 1 - 4 Petal Configuration

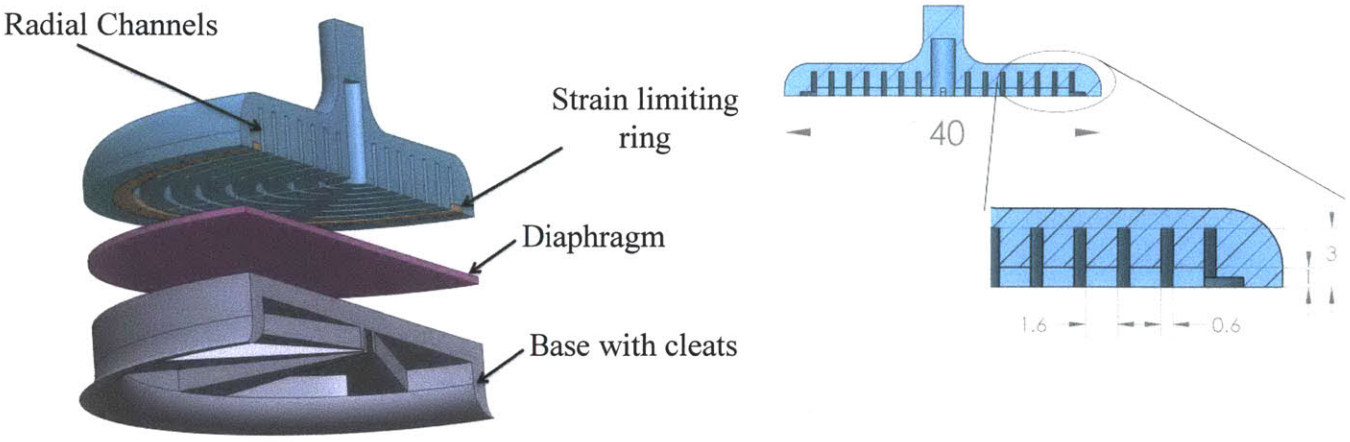

Figure 2.10: The CAD model of the cup and different components are shown (left) and the cross section view and the critical dimensions (right).

The radial channels have rectangular cross sections and are all interconnected through two intercrossing channels that connect all the radial channels together. This allows the air inserted into the channels to spread evenly. The desired deformation should occur at the top (compliant layer) and bottom surface of the PPAS. The diaphragm is simply used as a manufacturing technique. Due to the complex geometry, the base must be over molded to the top PPAS. However, the uncured over-mold rubber would easily flow up and block the channels if the openings on the bottom of the channels are not sealed. The diaphragm is a thin layer of silicon rubber over-mold to seal the channels completely. The cleats feature on the bottom of the base is used to minimize the amount of contact force achieved when pressed against a surface.

EcoFlex is a very soft and sticky material and adhere to smooth surfaces easily by Van der Waals force. In order to test the concept and isolate the functionality of "Positive Pressure Actuation", the minimization of other adhering forces was necessary. The strain limiting ring is made from a type of polyurethane rubber, VytaFlex 60. Because there are very few ways to adhere silicon rubber to urethane, the method of over-molding was used in order to place the strain limiting ring at the position indicated in the model above.

2.3.2 Prototype 2 - Spiral configuration

Unlike the four-petal configuration, the spiral configuration connects the channels through a winding spiral. This allows the flow of air to go from the stem to the circumference evenly without adding the intercrossing channels to connect the radial channels. The spiral configuration allows for a larger deformation area, but has the same diameter have the four petal configuration.

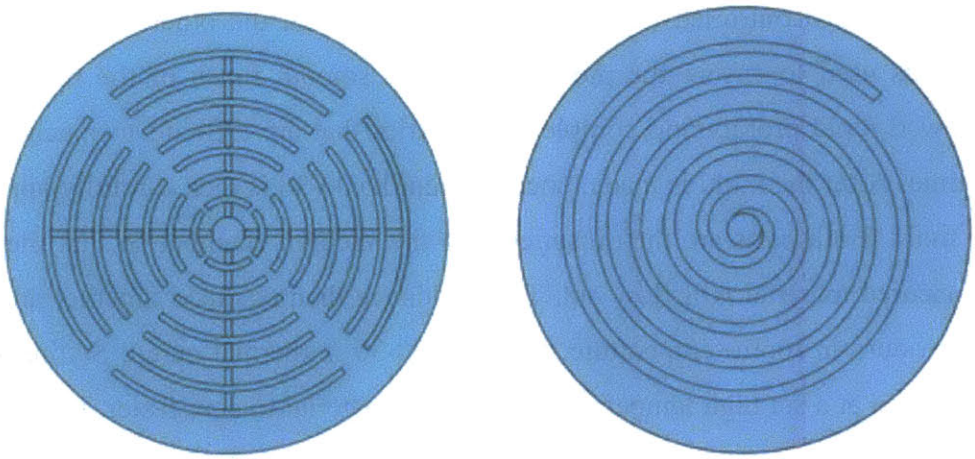

Figure 2.11: Channel cross-section view of four-petal (left) and spiral configuration (right)

2.3.3 Prototype 4 - Two flap configuration

The weakest part of the suction cup is the flaps around the circumference. When the PPAS is pulled away from the contact surface, it is the flap that deforms and fails first. The two-flap configuration is to see if multiple flaps will be able to create a better seal than having a single flap. The inner flap is designed to be 0.25 mm longer than the outer flap such that when

the outer flap breaks from the seal with the contact surface, the inner flap will still be able to keep the seal.

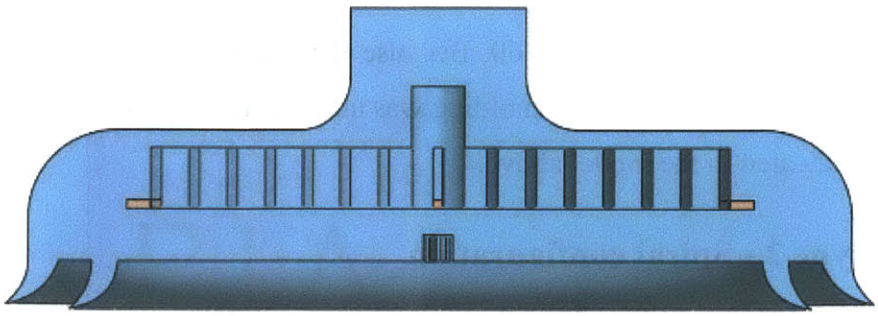

Figure 2.12: Two-flap configuration

2.4 Fabrication Process

Multiple molding processes are required to produce the entire PPAS assembly. First, the top part of PPAS is molded using two part mold, in which one part is machined out of delrin on a Computer Numerical Controlled (CNC) milling machine and the other is 3-D printed out of ABS. CNC was used to ensure the precision and the smooth finish of the molded part. 3-D printing allowed rapid prototyping complex geometries that are difficult to machine in a short amount of time. After the mold is made, uncured EcoFlex00-30 is then carefully applied on both part of the mold. Both parts are then inserted into the vacuum chamber so that the air bubbles within the uncured material will flow out. The molds are then clamped together and allowed to cure for four hours in room temperature. EcoFlex 00-30 is thermal cured. Setting the uncured sample in an oven at a set high temperature allows the material to cure faster. However, because the mold is enclosed in a volume with very limited access to air, the cure was sometimes much slower than expected. For consistency, at least four hours was given to cure.

Next, a very thin layer of EcoFlex 00-30 diaphragm is poured on a flat surface and left to flatten itself using gravity. The only purpose of the diaphragm is that when the base is over molded onto the top part, the uncured material does not flow up the channels and block the air flow passage ways. The diaphragm is over molded onto the top with the strain limiting ring placed inside the top. After this layer has cured, the base is then over molded onto the diaphragm.

Mold release is used on parts of the mold that are 3-D printed due to the rough texture of the printed molds. Ethylene was also used to clean the cured part such that the over molding procedure can adhere the two parts cured at different times together.

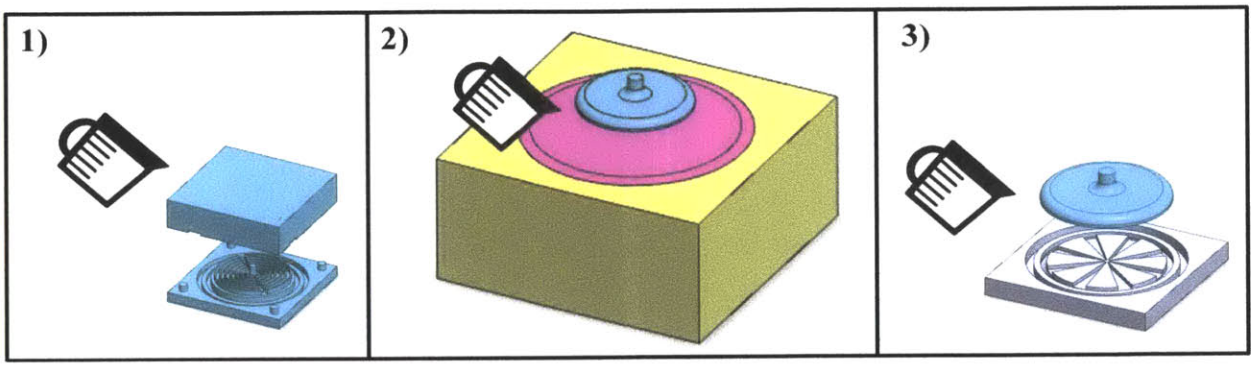

Figure 2.13: Molding Process of PPAS

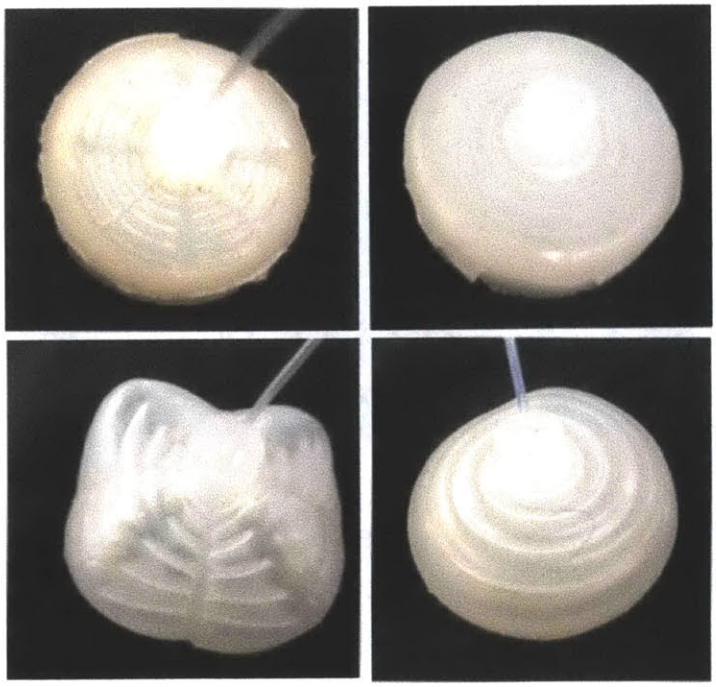

Figure 2.14: : The initial and actuated conditions of four-petal and spiral configuration

Chapter

3

EXPERIMENTS AND DISCUSSION

3.1 Experimental Setup

A variety of experiments were conducted to understand the behavior of the system. The pressure was measured both inside the channels and under the PPAS after the flaps have achieved a seal with the contact surface. An experiment was also done to find the maximum force PPAS can be pulled normal to the contact surface before failure.

The experiments were executed using two pressure sensors as shown in Figure 3.1. To measure the positive pressure (gauge) within the channels, a Honeywell MPXH6400A pressure sensor was hooked up to the syringe that is used to insert air into the channels. The syringe becomes the actuator that causes a positive pressure differential in the channels, which deforms the suction cup geometry and creates suction. To measure the pressure that is under the PPAS, a pressure sensor, Motorola MPX5999D, was attached to the bottom of a delrin plate with air-tight putty material. National Instruments (NI) – USB6211 DAQ system and NI LabView was used to collect data. Experiments includes seeing how the amount of air inserted affects the pressure differential inside the channels, how increasing the load on the PPAS affects the pressure differential under the cup, and how much load the PPAS is capable of taking before failure.

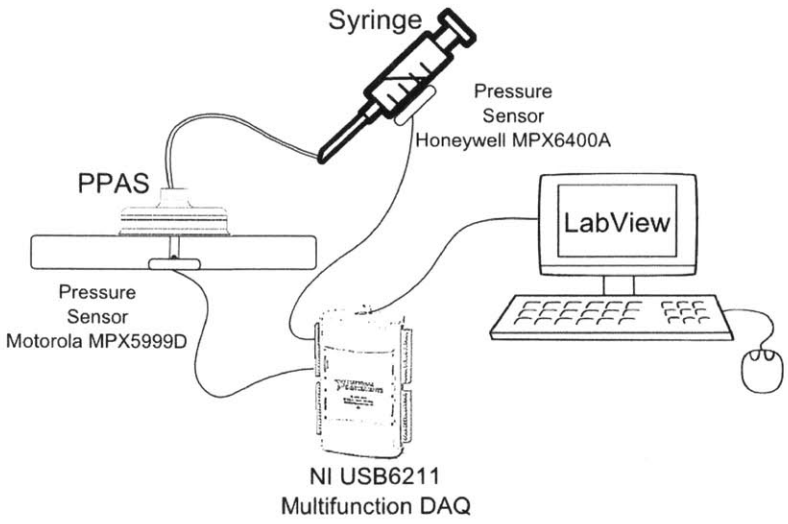

Figure 3.1: Experimental setup with two pressure sensors

For all the experiments, the range for the air volume insertion was set to be from 0 mL to 10 mL. This is because the top layer of the prototype is thin enough that when more than 10 mL of air is inserted, the increased strain on the top layer may cause it to tear. Load was applied on the suction cup by pulling the prototype in the direction normal to the contacting surface.

3.2 Results and Discussion

3.2.1 Channel Pressure

Channel pressure increases as gas is inserted into PPAS. The channel pressure increases linearly for the first 5 mL of air inserted. Then, the suction cup starts to deform dramatically and the channel pressure plateaus. This shows that the load applied to the suction cup from the pressure created by inserting air has exceeded the linear deformation regime in the silicon rubber material. Though more volume of air is inserted, the pressure is not being built up. This is because the material is expanding, therefore increasing the channel volume within PPAS, keeping the pressure level. The material deforms more during the 6 mL-10 mL volume insertion regime to compensate for the lack of increase in pressure within the channels.

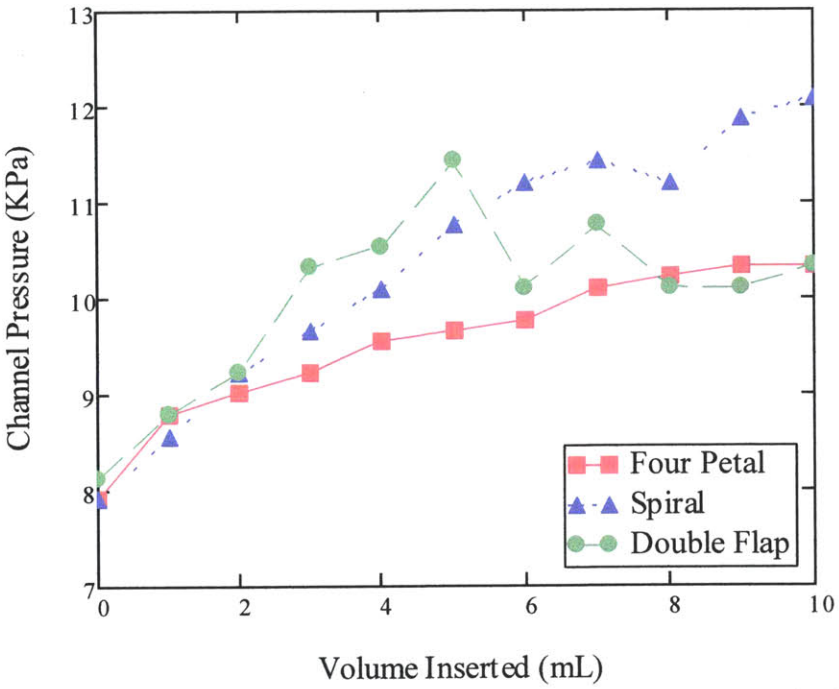

Figure 3.2: Volume Inserted vs. Channel Pressure during Pneumatic Actuation

3.2.2 Failure Load

To test how the deformation of PPAS affect the suction force, an experiment was executed to measure the failure load at which the PPAS detaches from the contact surface. 0 mL, 5 mL and 10 mL of air was first inserted into the prototype; then the prototype was manually pulled upwards in the direction normal to the contact surface until the seal is broken. As more volume is inserted into the prototype, the material should have expanded more and therefore, have increased the volume between the bottom layer of the prototype and the contact surface. The pressure at which the PPAS detached from the contact surface is recorded as the failure load, which is equivalent to the suction force of the PPAS prototype.

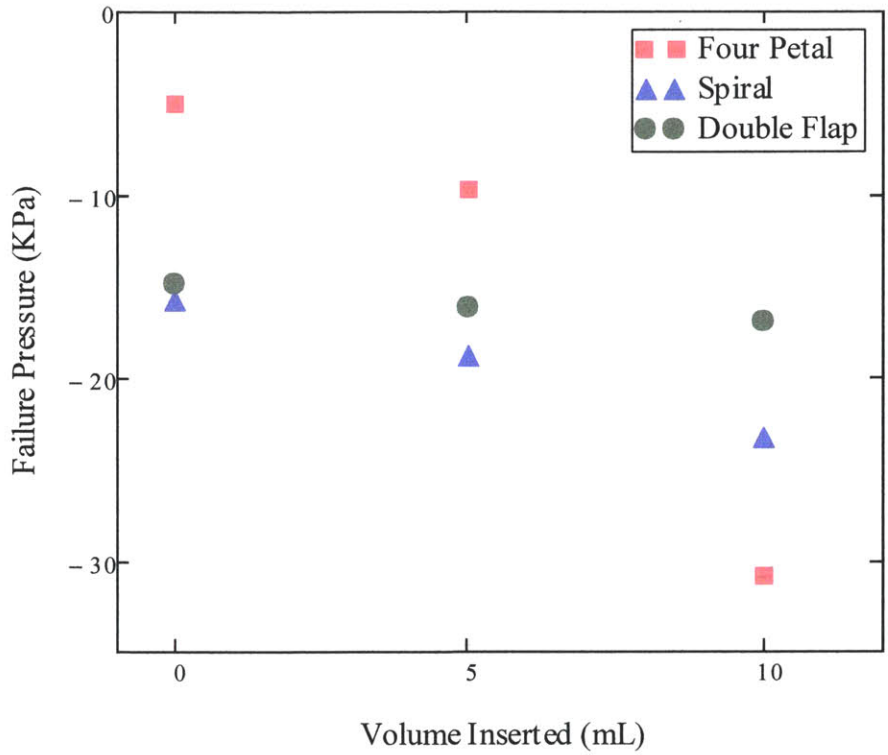

Figure 3.3: Volume Inserted vs. Failure Load

The failure load is expressed as negative pressure in relationship to atmospheric pressure. Because there is a negative pressure differential under the PPAS, there is a suction force that is pressing the prototype on to the contact surface. As expected, the absolute value of the failure load increased as the insertion volume increased. From the data points given, we are unable to conclude a mathematical relationship between the two variables. However, the direct relationship is clearly demonstrated.

The maximum suction force each prototype can sustain is described in the Table 3.1. There is a significant difference in the variation of force between a pneumatically actuated and non-actuated PPAS.

Table 3.1: Failure Load at Insertion Volume 10mL

	Failure Load (N)		
Volume Inserted	Four petal	Spiral	Double Flap
0mL	8.0	25.1	23.9
10mL	68.1	51.4	37.4

Figure 3.4 shows the relationship between suction pressure, which is the pressure that is under the PPAS when a surface seal is already established and channel pressure. Both are shown as gauge pressure. From approximately 2- 4 seconds, 10 mL of air is inserted into the prototype. The channel pressure increases rapidly during this time. From 5-10 seconds, the suction cup is pulled away from contact surface, therefore increasing the magnitude of suction pressure rapidly. At approximately 12 seconds, the surface seal is broken due to the applied load on the suction cup, and suction pressure magnitude decreases. The graph shows that both pressure in channels and under the suction cup returns to un-actuated state because the connection tubing between the pneumatic actuation (syringe) and the PPAS prototype disconnected at the time of load failure. The channel pressure should not change at the time the PPAS flap loose contact with contact surface. This is exemplified for the double flap channel pressure in Figure 3.5.

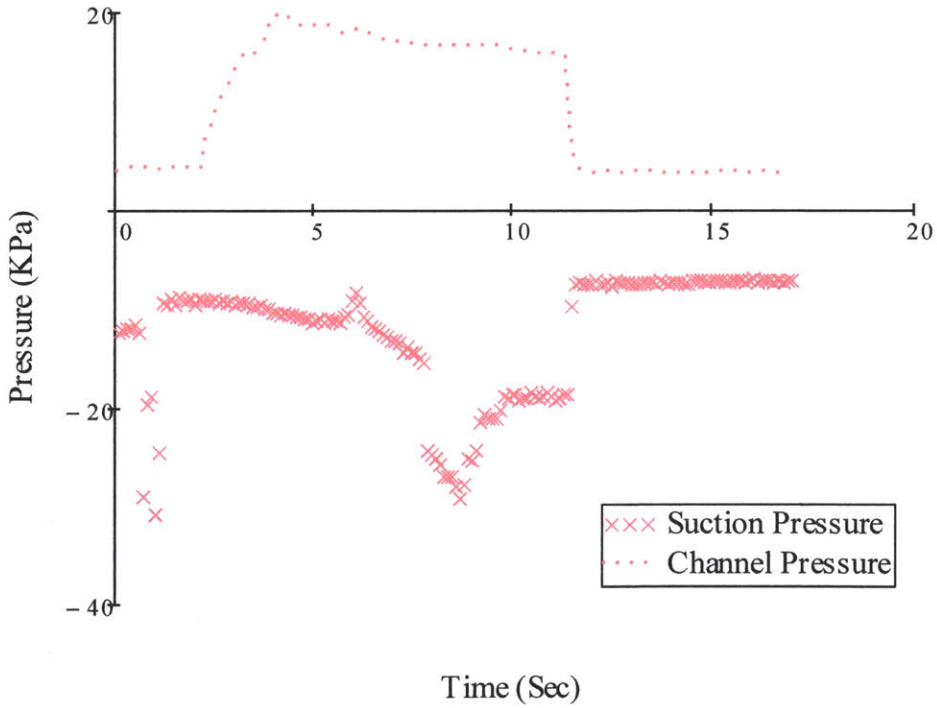

Figure 3.4: Volume Inserted vs. Failure Load for Four Petal Configuration

The pressure measured does not start at 0 because before air is inserted, PPAS is first pushed onto the contact surface to establish a good seal around the circumference of the PPAS. As shown in Figure 3.5, the starting pressure is different for all prototypes because there is a variable amount of suction force is established at the beginning when creating a seal with the contact surface.

Figure 3.5 compares the pressure data of the three different prototypes made. The double flap configuration achieved the highest channel pressure and the double flap configuration achieved the highest suction force (directly related to suction pressure). The spiral configuration sustained a larger positive pressure differential compared to other prototypes, which means that when the same amount of air was inserted, the elastomer did not extend as much on average. It is interesting to note that though the spiral configuration had a larger deformation area, stated in Table 2.4, it expanded less.

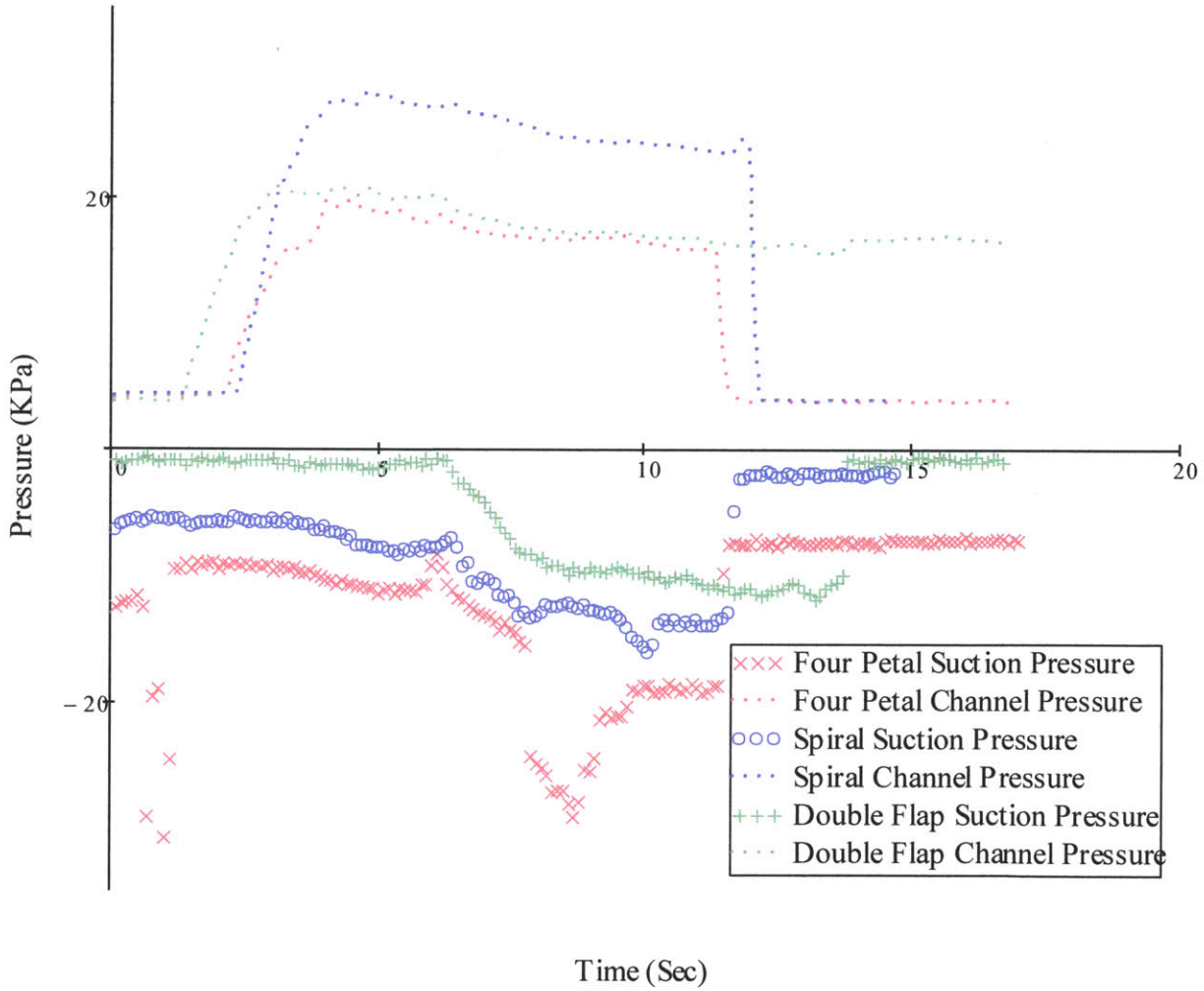

Figure 3.5: Volume Inserted vs. Failure Load for all configurations

The failure mechanism of the system is consistently at the contact surface where the flap of the PPAS touches the delrin surface. When the seal is broken, it is because the circumferential flap is creased and folded in a way that it is no longer flat against the delrin surface. The design

required the flaps to be as thin and compliant as possible, however, this feature was very hard to de-mold in a clean way after the material have cured. The flap circumferential shrinkage is shown in Figure 3.6.

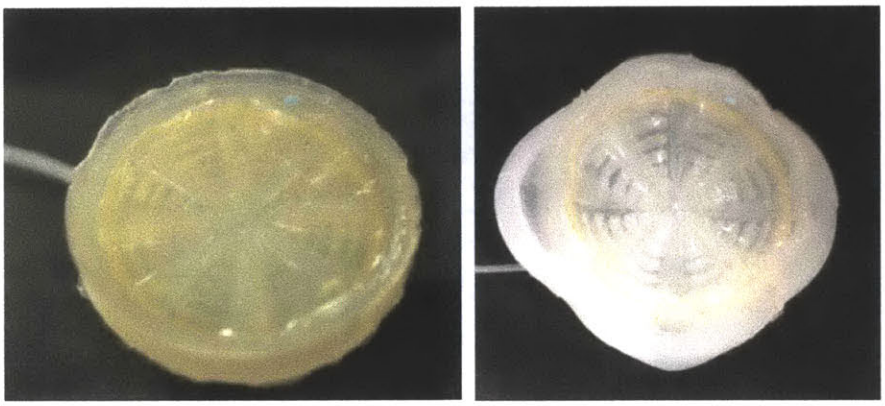

Figure 3.6: Bottom view of four petal configuration at initial and actuated state

Chapter 4

CONCLUSION

4.1 Conclusion

The purpose of this research is to explore an adhesive method of achieving high traction for a robotic foot along the inner surface of pipes. Suction is a mechanism that uses pressure differentials to establish a force that keeps the suction cup and the surface attached. However, active suction often requires a pump, which is heavy and costly. This paper explores an alternative way to actuate suction using compressive hydraulics. Rather than directly pulling fluid out to create a negative pressure differential, the PPAS is deformed to increase the volume underneath the suction cup, which directly causes a decrease in pressure. The goal is to be able to actuate suction cups using pneumatic/hydraulic actuators fast and reliably. Through creating a general mathematical model for the PPAS, simulating the model behavior in FEA ABAQUS 6.10, designing and fabricating multiple prototypes and measuring the pressure and suction force corresponding to each design, the PPAS concept is proved to be capable of taking on loads as much as 68 N. Experiments also show that the larger volume of air is inserted into the channels of PPAS, the larger the magnitude of the failure suction load. Failure is consistently caused by the creasing and folding of the flaps as the suction cup is actuated and deformed.

4.2 Future Work

This paper has proved that a pneumatic actuation of a channeled suction cup can indeed sustain a reasonable suction force. However, many detailed analysis and various geometry explorations were not done. A direct mathematical relationship between volume inserted and suction force, corresponding to a variety of channel geometry, would be helpful in controlling the adherence precisely. The suction force is expected to increase in an exponential way because the nonlinear regime of the material suggests that the strain increases as more volume of air is inserted. The greater the expansion, the larger the volume should be under the PPAS, which should directly affect the suction force. The failure mechanism that breaks the seal is consistently at where the flap contacts the surface. This shows that if the flap can sustain a seal, the maximum suction force capable of being maintained could be much greater than the results obtained. Further prototypes can be explored with different geometry around the flaps to secure the seal even during actuation. The shear force should also be explored. Eventually the experiments should be done underwater to prove that the system behaves consistently when completely submerged in water.

REFERENCES

[1] Zhang, Y., and Yan, G., In-pipe Inspection Robot with Active Pipe-diameter Adaptability and Automatic Tractive Force Adjusting, *Mechanism and Machine Theory,* vol. 42, issue 12, pp. 1618-1631, 2007.

[2] H.T. Roman, B.A. Pellegrino, "Pipe crawling inspection robots: an overview", *IEEE Transactions on Energy Conversion*, 1993

[3] M. Beller, E. Holden, N. Uzelac, "Cracks in pipelines and how to find them", Pipe and Pipelines International 2001, pp. 26–34

[4] S. Hirose, H. Ohno, T. Mitsui, "Design of in-pipe inspection vehicles for B25, B50, B150 pipes", *IEEE International Conference on Robotics and Automation* 1999, pp. 2309–2314.

[5] M. Muramatsu, N. Namiki, R. Koyama, "Autonomous mobile robot in pipe for piping operations", *IEEE/RSJ International Conference on Intelligent Robots and Systems*, 2000, pp. 2166–2171.

[6] H.R. Choi, S.M. Ryew, "Robotic system with active steering capability for internal inspection of urban gas pipelines", *Mechatronics,* 2002, pp.713–736.

[7] J. M. Mirats Tur, W. Garthwaite, "Robotic Devices for Water Main In-Pipe Inspection," *Journal of Field Robotics, 2010*

[8] Changrak, C., Chatzigeorgiou, D., Ben-Mansour, R., and Youcef-Toumi, K., Design and Analysis of Novel Friction Controlling Mechanism with Minimal Energy for In-pipe Robot Applications, Proc. of *IEEE International Conference on Robotics and Automation* , 14-18 May 2012, St. Paul, MN, USA, pp.4118-4123.

[9] Peng, L., Shugen, Ma., Bin, L., Yuechao, Wang., and Yunhui, Liu., Self-rescue Mechanism for Screw Drive In-pipe Robots, *Proc. of IEEE/RSJ International Conference on Intelligent Robots and Systems,* 18-22 October 2010, pp.2843-2849.

[10] S. Kim, M. Spenko, S. Trujillo, B. Heyneman, D. Santos, M.R. Cutkosky. Smooth Vertical Surface Climbing with Directional Adhesion. IEEE a special issue of transactions on Bio-Robotics, 24(1):65-74, Feb 2008.

[11] Y. Yoshida, S. Ma, "Design of a Wall-Climbing robot with passive Suction Cups", *IEEE Conf. on Robotics and Biomimetic,* Tianjin, China, Dec. 2010 pp. 1513-1518

[12] B.P. Epps, "Swimming performance of a biomimetic compliant fish-like robot", *Exp Fluids,* Vol. 47, pp. 927-939, 2009

[13] C. C. Kessens, J. P. Desai, "Design, Fabrication and Implementation of Self-sealing Suction Cup Arrays for Grasping", *IEEE Conf. on Robotics and Automation, Anchorage, Alaska* , May 2010 pp. 765-770

[14] B Mazzolai, et al, "Soft-robotic arm inspired by the octopus: II. From artificial requirements to innovative technological solutions", *IOP Bioinspir. Biomim. 7 (2012)*

[15] R.F. Shepherd, et al, "Multigait soft robot" *PNAS* Vol. 108, No.51, 2011

[16] D Tepayotl-Ramirez, T. Lu, Y, Park, and C. Majidi, "Collapse of triangular channels in soft elastomer", *Appl. Phys. Lett. 102, 044102 (2013)*

[17] B. Kim, et al. "A Comparison Among Neo-Hookean Model, mooney-Rivlin Model, and Odgen model for Chloroprene Rubber", *International Journal of Precision engineering and Manufacturing,* Vol. 13, No. 5, pp. 759-564, 2012

[18] Mooney, M., "*A Theory of Large Elastic Deformation*," Journal of Applied Physics, Vol. 11, No. 9, pp. 582-591, 1940.

[19] Rivlin, R. S., *"Large Elastic Deformations Isotropic Materials. IV. Further Developments of the General Theory,"* Philosophical Transactions of the Royal Society A, Vol. 241, No. 835, pp. 379-397, 1948.

[20] A. Atieh , et al, "FEM Analysis of the Interaction between a Piezoresistive Tactile Sensor and Biological Tissues," *International Conference on Bioinformatics, Computational Biology and Biomedical Engineering* 2011

APPENDIX

A

PPAS DIAGRAM

A.1 PPAS Structure Diagram

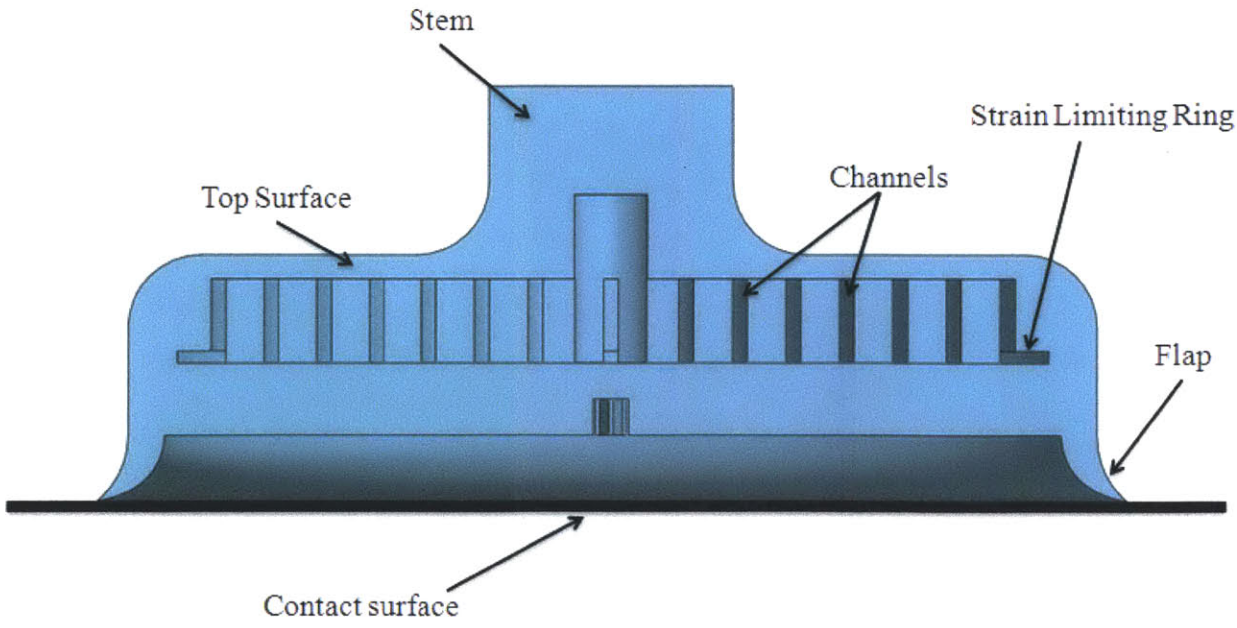

Figure A.1: PPAS Structure Diagram